Am J Physiol Lung Cell Mol Physiol 305: L322–L332, 2013.
First published June 28, 2013; doi:10.1152/ajplung.00424.2012.

Wt1-expressing progenitors contribute to multiple tissues in the developing lung

Elena Cano,* Rita Carmona,* and Ramón Muñoz-Chápuli

Department of Animal Biology, Faculty of Sciences, University of Málaga, Málaga, Spain

Submitted 21 December 2012; accepted in final form 23 June 2013

Cano E, Carmona R, Muñoz-Chápuli R. Wt1-expressing progenitors contribute to multiple tissues in the developing lung. *Am J Physiol Lung Cell Mol Physiol* 305: L322–L332, 2013. First published June 28, 2013; doi:10.1152/ajplung.00424.2012.—Lungs develop from paired endodermal outgrowths surrounded by a mesodermal mesenchyme. Part of this mesenchyme arises from epithelial-mesenchymal transition of the mesothelium that lines the pulmonary buds. Previous studies have shown that this mesothelium-derived mesenchyme contributes to the smooth muscle of the pulmonary vessels, but its significance for lung morphogenesis and its developmental fate are still little known. We have studied this issue using the transgenic mouse model mWt1/IRES/GFP-Cre ($Wt1^{cre}$) crossed with the Rosa26R-EYFP reporter mouse. In the developing lungs, *Wt1*, the Wilms' tumor suppressor gene, is specifically expressed in the embryonic mesothelium. In the embryos obtained from the crossbreeding, the *Wt1*-expressing cell lineage produces the yellow fluorescent protein (YFP), allowing for colocalization with differentiation markers. $Wt1^{cre}$-YFP cells were very abundant from the origin of the lung buds to postnatal stages, contributing significantly to pulmonary endothelial and smooth muscle cells, bronchial musculature, tracheal and bronchial cartilage, as well as $CD34^+$ fibroblast-like interstitial cells. Thus $Wt1^{cre}$-YFP mesenchymal cells show the very same differentiation potential as the splanchnopleural mesenchyme surrounding the lung buds. $FSP1^+$ fibroblast-like cells were always YFP^-; they expressed the common leukocyte antigen CD45 and were apparently recruited from circulating progenitors. We have also found defects in pulmonary development in $Wt1^{-/-}$ embryos, which showed abnormally fused lung lobes, round-shaped and reduced pleural cavities, and diaphragmatic hernia. Our results suggest a novel role for the embryonic mesothelium-derived cells in lung morphogenesis and involve the Wilms' tumor suppressor gene in the development of this organ.

pulmonary development; coelomic epithelium; mesothelium; Wilms' tumor suppressor gene

THE DEVELOPMENT OF THE RESPIRATORY system was a key evolutionary event for the air-breathing vertebrates. Lungs arose as specialized endodermal sacs from the digestive tract, and this phylogenetic origin is recapitulated in lung ontogeny. The contribution of mesodermal cells to the endodermal structures is essential for pulmonary development and function. In mouse embryos, the lung primordium sprouts from the ventral foregut by embryonic day (E) 9.5. It consists of a simple tube of endodermal epithelium surrounded by mesenchyme derived from the splanchnic mesoderm and lined by a layer of mesothelium. This primary tube branches in the pair of pulmonary sacs (reviewed in Ref. 17).

Pulmonary mesenchyme is essential for vascularization of the lungs. This process starts very early, around E10.5, once the systemic circulation has been established. Lung vascularization has been carefully described (10, 11). Primitive capillary formation begins in the periphery of the lung by a process of vasculogenesis, i.e., migration and coalescence of angioblasts that will form vessels. During midgestation vascular growth is carried out by angiogenesis (1, 30, 36). Besides this role in the vascularization of the lungs, the pulmonary mesenchyme also plays a fundamental role in lung morphogenesis given that this process is dependent on the crossed signals between endoderm and mesenchyme (6, 38, 40). Endodermal Shh signals promote the proliferation of the mesenchyme, acting as a potent mitogen (3, 12, 23). Fgf-10 is expressed in the splanchnic mesoderm surrounding buds in early stages of lung development and is essential for their formation (5, 37, 41). Fgf-9 is expressed in the endodermal and coelomic epithelia, and it promotes proliferation of the mesenchyme, regulates Fgf-10, and maintains the Shh signal (38). The null mutants for Fgf-10 and Fgf-9 die after birth with severe pulmonary defects (8, 26, 37, 43). In all these studies, the pulmonary mesenchyme is considered an homogeneous population at least from the point of view of its mesodermal origin. However, at least an additional source of pulmonary mesenchyme has been demonstrated, originating through delamination of cells from the mesothelium lining the lung buds through an epithelial-mesenchymal transition (35). This process has been described in other organs such as the heart (25, 31, 32), the liver (19), or the intestine (7). With the exception of the vascular smooth muscle (35), the contribution of this alternative source of mesenchyme to the different tissues of the developing lungs remains undetermined.

Since the Wilms' tumor suppressor gene *Wt1* is specifically expressed in the embryonic mesothelium of the lung buds since their inception (35), this gene is a reliable marker for the lineage of the cells derived from the mesothelium. We have developed a model based on the same Wt1-Cre system from other studies (9a, 42) using the Rosa26R-EYFP mouse line as a reporter. Yellow fluorescent protein (YFP) is highly expressed in all the Wt1-expressing cell lineage (that we will call herein $Wt1^{cre}$-YFP cells) and it could be easily colocalized with a number of cell differentiation markers. In this way, we have analyzed the fate and differentiation of cells derived from the coelomic mesothelium and their contribution to different pulmonary tissues. Since we have found that this contribution is quantitatively relevant, we have also studied the lung phenotype of the $Wt1^{-/-}$ mouse embryos, and we have found hitherto undescribed defects that suggest a key role for Wt1 in pulmonary morphogenesis.

* E. Cano and R. Carmona contributed equally to this paper.

Address for reprint requests and other correspondence: R. Muñoz-Chápuli, Dept. of Animal Biology, Faculty of Sciences, Univ. of Málaga, 29071 Málaga, Spain (e-mail: chapuli@uma.es).

Table 1. *Detail of the antibodies used in this study*

Antigen	Manufacturer	Host Animal	Labeling
α−SMC-Actin	Sigma #A2547	Mouse monoclonal	Indirect Cy5 or TRITC
B-Galactosidase	Cappel #55976	Rabbit polyclonal	Indirect, FITC
CD31 (PECAM-1)	Pharmingen #550274	Rat monoclonal	Indirect, Cy5
CD34	eBioscience #50-0341-80	Rat monoclonal	Direct, eFluor 660
CD45	eBioscience #12-0451-81	Rat monoclonal	Direct, Phycoerythrin
CD117	DAKO #A4502	Rabbit polyclonal	Indirect, Cy5
FGF9	Antigenics #RMF324	Rabbit polyclonal	Indirect, Cy5
FSP1	Gift from Dr. Eric Neilson (Univ. Vanderbilt)	Rabbit polyclonal	Indirect, Cy5
PH3	Upstate #06570	Rabbit polyclonal	Indirect, Cy5
Sca-1	Biolegend #122517	Mouse monoclonal	Direct, Cy5
Wt1	Sta. Cruz #Sc-192	Rabbit polyclonal	Indirect, Peroxidase

MATERIALS AND METHODS

The animals used in our research program were handled in compliance with the institutional and European Union guidelines for animal care and welfare. The procedure was approved by the Committee on the Ethics of Animal Experiments of the University of Málaga (procedure code 2009-0037). The mWt1/IRES/GFP-Cre ($Wt1^{Cre}$) mouse has been used for previous studies of the Wt1 lineage (22, 37). Homozygote ($Cre^{+/+}$) mice were crossed with Rosa26R-EYFP [B6.129X1-Gt(ROSA)26Sortm1(EYFP)Cos/J]. The WT470LacZ mice strain expressing LacZ under control of the human WT1 promoter was generated as previously described (28). The Wt1 GFP/$^{+}$ knockin line (18), in which the exon 1 of one Wt1 allele has been replaced by the GFP sequence, was also used as reporter of the Wt1 expression. Wt1 knockout mice ($Wt1^{-/-}$) were generated by gene targeting, as previously described (21).

Immunofluorescence and immunohistochemistry. Embryos were staged from the time point of vaginal plug observation, which was designated as the stage E0.5. Whole embryos and the viscera of neonates were excised, washed in PBS, and fixed in 4% fresh paraformaldehyde solution in PBS for 2–8 h. Then the embryos were washed in PBS, cryoprotected in sucrose solutions, embedded in OCT, and frozen in liquid N_2-cooled isopentane, and 10-μm cryosections were stored at −20°C until use.

Embryos that were used for immunohistochemistry with the polyclonal antibody Wt1 were frozen unfixed in liquid N_2-cooled isopentane, and 10-μm cryosections were cut on a cryostat. Before immunostaining, the sections were fixed with methanol/acetone 1:1 at −20°C for 10 min.

For immunofluorescence and immunohistochemistry, cryosections were rehydrated in Tris-PBS (TPBS) and blocked for nonspecific binding with 16% sheep serum, 1% bovine albumin, and 0.1% Triton X-100 in TPBS. Primary antibodies used are detailed in Table 1. When biotinylated secondary antibodies were used, endogenous biotin was blocked with the Avidin-Biotin blocking kit from Vector.

Single immunofluorescence was performed by incubating the sections with the primary antibody overnight at 4°C, washing in TPBS, and incubating with the corresponding fluorochrome-conjugated secondary antibody for 1 h at room temperature. Secondary antibodies were not used in the case of the anti-CD34 and anti-CD45 antibodies, which were conjugated to eFluor660 and phycoerythrin, respectively. Nuclei were counterstained with DAPI (Sigma). Double immunofluorescence was performed by mixing both primary antibodies (rabbit polyclonal and mouse or rat monoclonal) and incubating overnight at 4°C. In the case of the double CD31/SMC-α-actin immunostaining we incubated overnight the sections with the anti-CD31 antibody, then we blocked the sections with monovalent donkey anti-mouse IgG, and we incubated the sections again with the anti-SMC-α-actin antibody, before incubation with fluorochrome-conjugated secondary antibodies. In the case of the double CD31/CD34 immunostaining we incubated the sections overnight with the anti-CD31 antibody, then with a biotin-conjugated anti-rat IgG antibody followed by incubation with TRITC-conjugated extravidin. We saturated the sections with rat IgG, and we finally incubated the sections with the eFluor660-conjugated anti-CD34 antibody. Negative controls were performed incubating with nonimmune rat, mouse, or rabbit IgG instead of the primary antibody.

WT1 immunohistochemistry was performed by incubating the sections with the primary rabbit anti-Wt1 antibody, a secondary biotinylated anti-rabbit IgG antibody, and extravidin-peroxidase. Staining of the sections was performed with a diaminobenzidine kit (Sigma-Aldrich).

Time-lapse microscopy. E11.5 $Wt1^{cre}$/ROSA26R-EYFP mouse embryos were dissected in PBS supplemented with 10% FBS, penicillin (100 U/ml) and streptomycin (100 μg/ml). Lung buds were

Fig. 1. Wt1 expression and Wt1-expressing cell lineage in developing lungs of $Wt1^{cre}$ × ROSA26R-YFP embryos. *A–C*: immunolocalization of Wt1 protein in lungs of embryonic day (E) 10.5 (*A*), E12.5 (*B*), and E14.5 (*C*) embryos. Wt1 is localized in the coelomic epithelium of the lungs in all these stages (arrow in *A*). Cells showing a weak Wt1 immunoreactivity can be seen apparently delaminating from the coelomic epithelium (arrowheads in *insets*). A, cardiac atrium; LL and RL, right and left lung buds, respectively; OE, esophagus. *D*: immunolocalization of β-galactosidase in an E14.5 embryo of the Wt470-LacZ mouse line. The expression of β-galactosidase is restricted to the pulmonary mesothelium. The endothelium is stained with the anti-CD31 antibody. *E*: immunolocalization of Wt1 protein (red) and green fluorescent protein (GFP; green) in an E12.5 embryo of a GFP/$^{+}$ mouse line where GFP is coexpressed with Wt1. Both markers appears only in the pulmonary mesothelium. *F*: a control Wt1-$Cre^{+/+}$; Rosa26R-$EYFP^{-/-}$ E11.5 embryo does not show detectable GFP fluorescence owing to the mWt1/IRES/GFP-Cre driver used in this study. *G*: immunolocalization of endothelial (CD31/Pecam-1) and smooth muscle (α-SMA, i.e., smooth muscle cell α-actin) markers in the lung of an E10.5 embryo. Smooth muscle cells are not observed in the developing lungs by this stage, but endothelial differentiation has already started. Some $CD31^{+}$ cells express yellow fluorescent protein (YFP; arrows). *H*: CD34 immunolocalization in the lung bud of an E10.5 embryo. Differentiation of endothelial cells is confirmed with this marker, which also colocalizes with YFP in some cells (arrow). *I*: double CD31 (blue)/CD34 (red) immunolocalization in the lung of an E10.5 embryo. All the $CD31^{+}$ cells are also $CD34^{+}$ and they appear in magenta. Note the colocalization with YFP (arrows). *J*: double CD31/SMC-α-actin immunostaining in an E12.5 embryo. This is the earliest stage at which smooth muscle was observed around the main bronchia. Some smooth muscle cells express YFP (arrows). Note the YFP^{+} coelomic epithelium of the lung. *K*: the vascular plexus of the lung is well developed by the stage E13.5, as demonstrated by CD31 immunolocalization. Double CD31/YFP staining is evident in a number of cells (arrows). *L*: a few $Wt1^{cre}$-YFP cells can be seen in the cartilaginous condensation of the trachea by the stage E13.5 (arrows). Scale bars = 25 μm, except for *A*, *C*, *D*, and *E* (50 μm) and *B* and *F* (100 μm).

isolated and transferred to HEPES-buffered DMEM-F12 supplemented with 2% FBS and penicillin-streptomycin. Lung buds were embedded into a 1.5 mg/ml collagen gel (BD Bioscience) in a glass-bottom culture dish (MatTek). Images were captured in a Leica SP5 confocal microscope every 10 min for 12 h. During the capture, the culture chamber was maintained at 37°C in a 5% CO_2 humidified atmosphere.

Flow cytometry. For flow cytometry analysis, lungs from $Wt1^{Cre}$/Rosa26R-EYFP neonates were excised, dissociated for 15 min at 37°C in prewarmed collagenase solution (0.1% in HBSS + 3 mM $CaCl_2$) (Sigma), and homogenized by repeated pipetting. Cell suspension was washed in PBS plus 2% FBS and 10 mM HEPES. Then cells were incubated on ice at the dark with Cy5-conjugated rat anti-mouse CD31, Alexa 660-conjugated rat anti-mouse CD34, and Cy5-conjugated rat anti-mouse Sca-1. After washing, the cells were analyzed in a MoFlo cell sorter. Damaged cells were excluded from the results by propidium iodide staining.

Image analysis. Quantification of $Wt1^{cre}$-YFP cell abundance was performed by splitting green (YFP) and blue (DAPI) channels and expressing the area of the YFP^+ spots as percentage of the total area occupied by the nuclei stained with DAPI. The measurements were made with ImageJ software. Three to four images were used for each

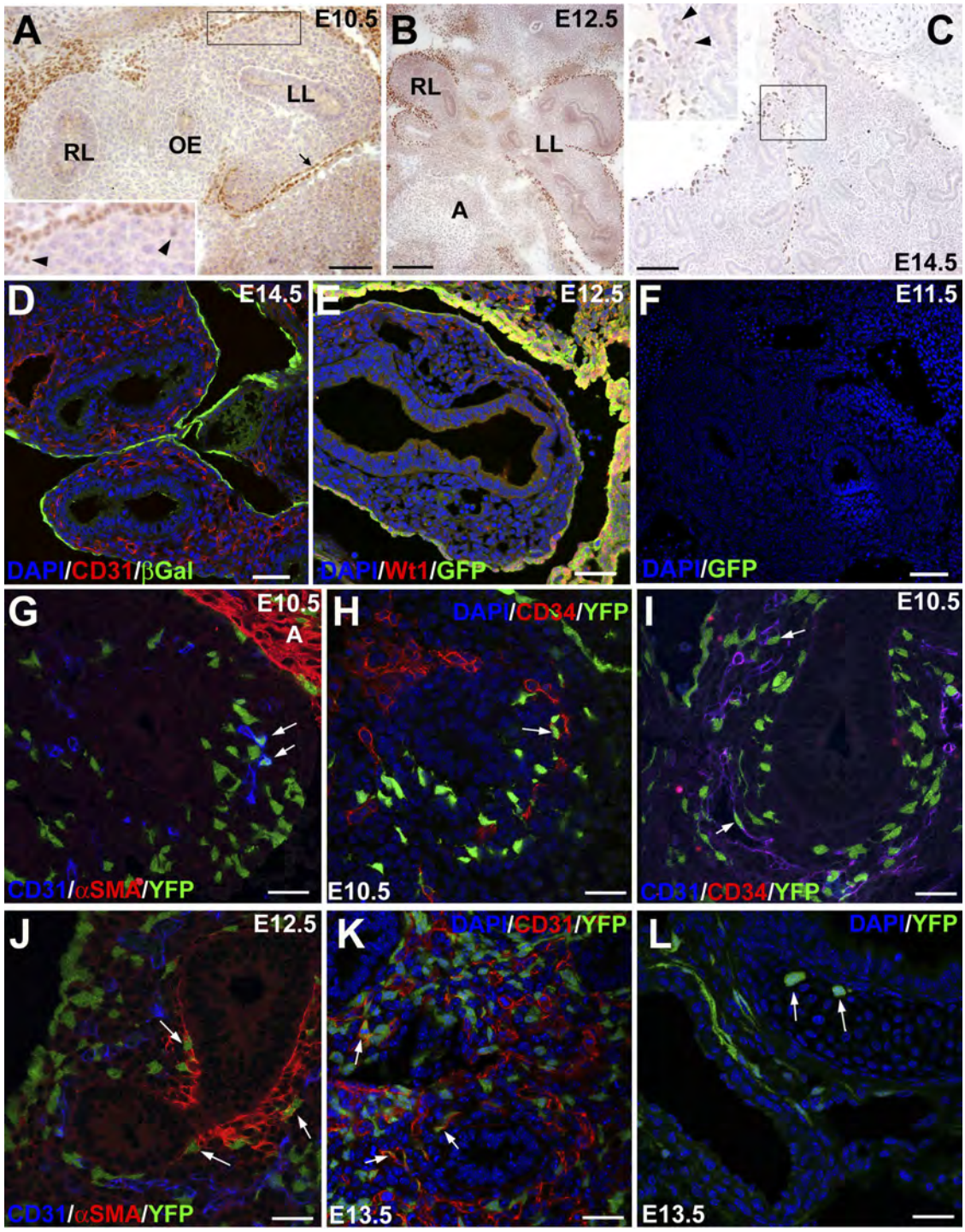

Table 2. *Quantitative analysis of Wt1^{cre}-YFP cells*

	E10.5	E12.5	E14.5	E16.5	E18.5	Neo
YFP$^+$ area/DAPI area (%)	20.53 ± 3.37	31.67 ± 2.07	42.37 ± 12.93	68.37 ± 11.54	42.57 ± 3.29	18.17 ± 6.02
YFP$^+$CD31$^+$/Total CD31$^+$ (%)	n.c.	8.67 ± 0.91	24.56 ± 12.14	26.57 ± 5.69	13.45 ± 2.12	n.c.

Flow cytometry analysis in neonates (percentage of total cells):

YFP$^+$ total (%) = 1.58 ± 0.51	YFP$^+$ total (%) = 1.83 ± 0.63	YFP$^+$ total (%) = 1.59 ± 0.37
CD31$^+$/YFP$^+$ (%) = 0.21 ± 0.09	CD34$^+$/YFP$^+$ (%) = 0.45 ± 0.07	Sca1$^+$/YFP$^+$ (%) = 0.25 ± 0.13
CD31$^+$/YFP$^-$ (%) = 6.66 ± 2.35	CD34$^+$/YFP$^-$ (%) = 8.59 ± 2.40	Sca1$^+$/YFP$^-$ (%) = 6.3 ± 2.04
CD31$^-$/YFP$^+$ (%) = 1.36 ± 0.55	CD34$^-$/YFP$^+$ (%) = 1.32 ± 0.62	Sca1$^-$/YFP$^+$ (%) = 1.34 ± 0.43
YFP$^+$ all experiments (%) = 1.67 ± 0.53		

The results of the quantification of Wt1^{cre}-YFP cells by image analysis and flow cytometry are expressed as means ± SE; n.c., not calculated. Neo, neonate.

developmental stage. The proportion of the Wt1^{cre}-YFP cells respect to the CD31$^+$ was calculated by manually counting double stained and single stained cells on three to four images for each developmental stage. All the results were expressed as means ± SE.

RESULTS

Wt1^{cre}-YFP cells contribute to early lung vascularization. At stage E10.5, Wt1 protein can be already localized by immunohistochemistry in the mesothelium surrounding the lung buds. A few cells with a weak staining are apparently migrating from the epithelium into the mesenchyme (Fig. 1*A* and *inset*). A similar immunoreactive pattern is observed 48 h later (Fig. 1*B*). At the stage E14.5, mesothelial cells also express Wt1, and signs of migration of cells showing weak Wt1 immunoreactivity are still detectable (Fig. 1*C* and *inset*). Despite this low level of Wt1 protein in the migrating cells, actual *Wt1* gene expression is restricted to the mesothelium, as demonstrated by the immunolocalization of β-galactosidase in the Wt470LacZ reporter (Fig. 1*D*). Immunolocalization of Wt1 protein in Wt1 GFP/$^+$ E12.5 embryos, where GFP is a reporter of the *Wt1* gene, also confirmed restricted expression of Wt1 to the mesothelium (Fig. 1*E*).

Since the Cre driver used (mWt1/IRES/GFP-Cre) induces the expression of low levels of GFP, we checked whether this expression could be interfering with the YFP expression of the reporter. Control Wt1-Cre$^{+/+}$; Rosa26R-EYFP$^{-/-}$ embryos show no detectable GFP levels in the lung tissue by confocal microscopy (Fig. 1*F*). Thus the green fluorescence detected in the tissues is exclusively attributable to the YFP reporter.

Wt1^{cre}/ROSA26R-EYFP E10.5 embryos show some Wt1^{cre}-YFP cells in the mesenchyme surrounding the endodermal epithelia, although their abundance is relatively low (Table 2). At this stage, the primary pulmonary vascular plexus is starting its formation, and a few Wt1^{cre}-YFP cells also expressed endothelial markers such as CD31 (Pecam-1) and CD34 (Fig. 1, *G* and *H*). They were not quantified because of their low abundance. Both markers always colocalized on the same cells (Fig. 1*I*). We did not observe α-SMC actin-expressing smooth muscle cells within the lung buds by this stage (Fig. 1*G*).

A more developed vascular plexus is present by the stages E12.5-E13.5 around the endodermal epithelium. As described in younger embryos, all the endothelial cells express both the CD31 and the CD34 markers (not shown). Colocalization of YFP with endothelial markers has become relatively frequent (Fig. 1, *J* and *K*) and reach ~9% of all the CD31$^+$ cells (Table 2). The earliest smooth muscle cells, identified by α-SMC actin immunoreactivity, appear at the stage E12.5 around the main bronchia. Some of these muscular cells are YFP$^+$ (Fig. 1*J*). Wt1^{cre}-YFP cells become very abundant by the stage E13.5, and they appear incorporated to the vessels (Fig. 1*K*) and to the mesenchymal condensations that will give rise to the tracheal cartilages (Fig. 1*L*).

The epithelial-mesenchymal transition of the pulmonary mesothelium was directly observed in Wt1^{cre}/ROSA26R-EYFP E11.5 embryos by time-lapse confocal microscopy of explanted lung buds (Fig. 2). YFP-expressing cells were observed clearly migrating from the mesothelium as the endodermal epithelium was growing and forming branches.

Wt1^{cre}-YFP cells contribute to the formation of airway and vascular smooth muscle in the developing lung. By midgestation, developing bronchia are composed of branched epithelial tubes surrounded by a thick layer of mesenchymal cells. A

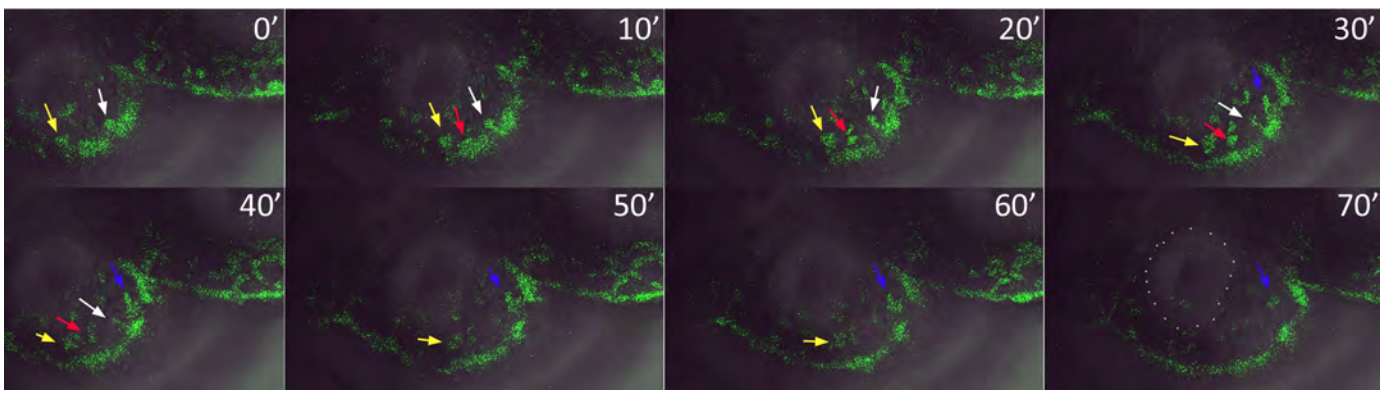

Fig. 2. Time lapse fluorescence microscopy of explanted Wt1^{cre} × ROSA26R-YFP lung buds. The series of images covers a period of 70 min. Color arrows indicate individual mesothelial cells that are migrating into the tissue as the endodermal sprout (marked with white dots in the last figure) grows.

highly developed vascular network is present throughout the lung. Wt1^{cre}-YFP cells can be found incorporated to the vascular endothelium of this network, expressing CD31 and CD34 (Fig. 3, *A*, *C*, and *D*). The relative abundance of Wt1^{cre}-YFP cells reaches its maximum by E16.5, although the proportion of the YFP$^+$/CD31$^+$ cells (~25% of all the endothelial cells) is about the same in E14.5 and E16.5 stages (Table 2). Airway and vascular smooth muscle can be identified by α-SMC actin immunoreactivity. In both cases, Wt1^{cre}-YFP cells appear incorporated to the smooth muscle layers (Fig. 3, *B* and *C*). The fibroblast marker FSP1 appears in cells of the developing lungs at the stage E16.5, but colocalization with YFP was not observed (Fig. 3*F*).

The presence of Wt1^{cre}-YFP cells in the vascular walls, including those from the large arteries and veins, is frequent by the end of the gestation (Fig. 3, *E*, *G*, and *H*). However, their relative abundance and their contribution to the vascular endothelium have decreased by E18.5 (Table 2).

Wt1^{cre}-YFP cells contribute to the pulmonary cartilage and also to CD34$^+$ fibroblast-like cells. In the latest gestational stages the microvascular endothelial cells are still expressing CD34, although the endothelium of more mature vessels shows a decrease in the expression of this marker (Fig. 3*E*). Furthermore, a number of CD34$^+$/CD31$^-$ fibroblast-like cells appear now in the pulmonary interstitium. Wt1^{cre}-YFP cells are frequently localized within this fibroblast-like cell population (Fig. 3, *E* and *I*). These CD34$^+$ cells were negative for the stem cell factor receptor c-Kit (Fig. 3, *K* and *L*). Wt1^{cre}-YFP rounded cells also appear within the cartilaginous condensations of the trachea and bronchi (Fig. 3, *I* and *J*). Chondrocytic differentiation of these Wt1^{cre}-YFP cells was confirmed with Alcian blue staining (Fig. 3*M*).

Wt1^{cre}-YFP cells are present in the lungs of neonates and adult mice. In neonates, Wt1^{cre}-YFP cells are still present in the lungs although their abundance has much decreased (Table 2). Some of them show expression of endothelial markers (Fig. 4, *A* and *B*), but the high abundance of CD31$^+$ cells in the neonatal lungs precluded quantification by image analysis. Thus we quantified them by flow cytometry as described below. The expression of the fibroblast marker FSP1 is now more abundant, but colocalization with YFP is very infrequent (Fig. 4*C*).

We analyzed sections of lungs of 3-mo-old Wt1^{cre}/ROSA-EYFP mice, where some Wt1^{cre}-YFP cells are still found. As in the embryos, Wt1^{cre}-YFP cells express CD31 and CD34, and many appear incorporated to the vasculature, but we could not find clear colocalization of YFP with FSP1 (Fig. 4, *D–F*).

Since FSP1 was not colocalized with YFP, suggesting a specific origin for the FSP1$^+$ cell population, we colocalized this marker with the leukocyte common antigen CD45. Most of the isolated FSP1$^+$ cells in E18.5 embryos and in neonates are CD45$^+$ (Fig. 4, *G–I*). Surprisingly, the tunica media of some arteries is also FSP1$^+$, but these smooth muscle cells are always YFP$^-$ (Fig. 4*G*).

We studied the proliferation of the Wt1^{cre}-YFP cells by colocalization with the marker of mitotic cells PH3 (phosphohistone-3) (Fig. 4, *J–L*). In E12.5 embryos, most proliferating Wt1^{cre}-YFP cells are located in the mesothelium (Fig. 4, *J* and *K*). Some YFP$^-$ endothelial cells are also positive for PH3 by this stage. However, in E18.5 embryos, PH3 immunoreactivity is scarce in the lungs, and it was not found in Wt1^{cre}-YFP nor in endothelial cells (Fig. 4*L*).

In neonates, colocalization of YFP with the endothelial markers CD31, CD34, and Sca-1 was quantified by flow cytometry analysis. A representative experiment is shown in Fig. 5, and the results of three different experiments are summarized in Table 2. In neonates, 1.67% of all the pulmonary cells were Wt1^{cre}-YFP. About 13% of this Wt1^{cre}-YFP cell population was CD31$^+$ and ~25% was CD34$^+$, confirming in this way the presence of CD34$^+$/CD31$^-$ cells. Fifteen percent of the Wt1^{cre}-YFP cells were also positive for the stem cell antigen Sca-1. These cells are probably endothelial, as discussed below.

Wt1$^{-/-}$ mouse embryos show abnormal lung development. Since cells from the Wt1 lineage demonstrated to account for a substantial fraction of the embryonic pulmonary mesenchyme, especially by midgestation, we decided to study the phenotype of the developing lungs in E13.5 mouse embryos with a loss of function of the *Wt1* gene. This is the most advanced stage that Wt1$^{-/-}$ embryos can reach in the genetic background that we used for this study. The gross morphology of the Wt1$^{-/-}$ lungs is anomalous, showing a rounded transverse section and abnormal fusion of the lobes (Fig. 6, *A*, *B*, *N*, and *O*). The accessory lobe is mislocated at the right of the mediastinum because of a defect in the pleuropericardic septum. A diaphragmatic defect is also evident, leading sometimes to pulmonary hernia (Fig. 6, *B* and *C*). The pleural cavities are also abnormal, small, round-shaped, and widely open to the

Fig. 3. Expression of vascular and fibroblastic markers in Wt1^{cre} × ROSA26R-YFP embryos. *A–C*: CD31 (*A*), SMC-α-actin (*B*), and double CD31/SMC-α-actin (*C*) immunolocalization in an E14.5 embryo. Some CD31$^+$ cells express YFP (arrows in *A*). Smooth muscle cells already appear around the pulmonary vessels. YFP expression is observed in endothelial and in smooth muscle cells, either vascular (arrowheads in *B*) or surrounding the developing bronchia (arrows in *B* and *C*). *D*: CD34 expression is very abundant in the pulmonary cells by the stage E15.5, when colocalization with YFP is frequent (arrows). *E*: by the stage E18.5, CD31 (red) and CD34 (blue) do not show a superposing pattern as in previous stages. Both antigens are present in microvessels (arrow), but CD34 immunoreactivity has decreased in the endothelium of the large vessels (arrowheads), and it appears in fibroblastoid cells that are CD31 negative (blue arrow). *F*: the fibroblastic marker FSP1 appears in cells of an E16.5 embryo (arrows). Colocalization of this marker with YFP was not observed. *G* and *H*: double CD31/SMC-α-actin immunostaining in an E18.5 embryo. By the end of the gestation, YFP$^+$ cells appear incorporated in the vascular walls of large vessels, either arteries or veins. Note the YFP$^+$ cells in the endothelium of a main artery (arrowheads in *G*) and in the muscular layer of the vein (arrow in *H*). A YFP$^+$ capillary is also shown in *H* (arrowhead). *I* and *J*: YFP$^+$ cells also appear in the cartilage of trachea and bronchia by the stage E18.5 (arrowheads). Note the CD34$^+$/CD31$^-$ cells surrounding the perichondrium of the trachea and the presence of YFP$^+$ cells in this population (arrow in *I*). *K*: double c-Kit (red)/CD34 (blue) staining in an E18.5 Wt1^{cre} × ROSA26R-YFP embryo. YFP label was found in the CD34$^+$ population (arrowheads) but not in the group of c-Kit$^+$ cells (arrow) located between 2 main bronchi (BR). Note the presence of YFP$^+$ cells in the endothelium of the artery (green arrows). *L*: positive control of the c-Kit immunolocalization performed in the esophagus. Cajal-like interstitial cells are abundant in the muscular layer and they show a strong c-Kit immunoreactivity (in red). Note the presence of abundant CD34$^+$/c-Kit$^-$ cells between the smooth muscle and the esophageal mucosa. Some of them are YFP$^+$ (arrowheads). *M*: superposition of Alcian blue staining with YFP fluorescence and CD34 immunolocalization (in red) in the lung of an E18.5 Wt1^{cre} × ROSA26R-YFP embryo. Alcian blue image was obtained by light microscopy, inverted, and color recoded to show positive cells in blue. Some chondrocytes (arrow) are YFP positive. Scale bars = 25 μm, except for *B*, *D*, *F*, *K*, *L*, and *M* (50 μm) and *I* (20 μm).

peritoneal cavity. The pleural walls are abnormally populated by cells (asterisks in Fig. 6, *A* and *B*). The pulmonary mesothelium of the mutant mice shows a complete basal lamina when stained with Sirius red. This continuous basal lamina is not observed in the control embryos (Fig. 6, *D* and *E*). The existence of the basal lamina in the mutant embryos was confirmed by laminin immunoreactivity (Fig. 6, *F* and *G*). Since this could suggest a blockade of the migration of cells from the mesothelium to the pulmonary mesenchyme, a process that involves degradation of the basal lamina, we checked the expression of vimentin, a mesenchymal marker, and we observed a much reduced number of vimentin-positive cells in the mutants compared with the control littermates. Additionally, the mesothelium of the control is vimentin immunoreactive, different from the mesothelium of the $Wt1^{-/-}$ lungs (Fig. 6, *H* and *I*). FGF9 immunoreactivity was also decreased in the mesenchyme and in the mesothelium of the mutant lungs. Expression in the pulmonary endodermal epithelium and in the

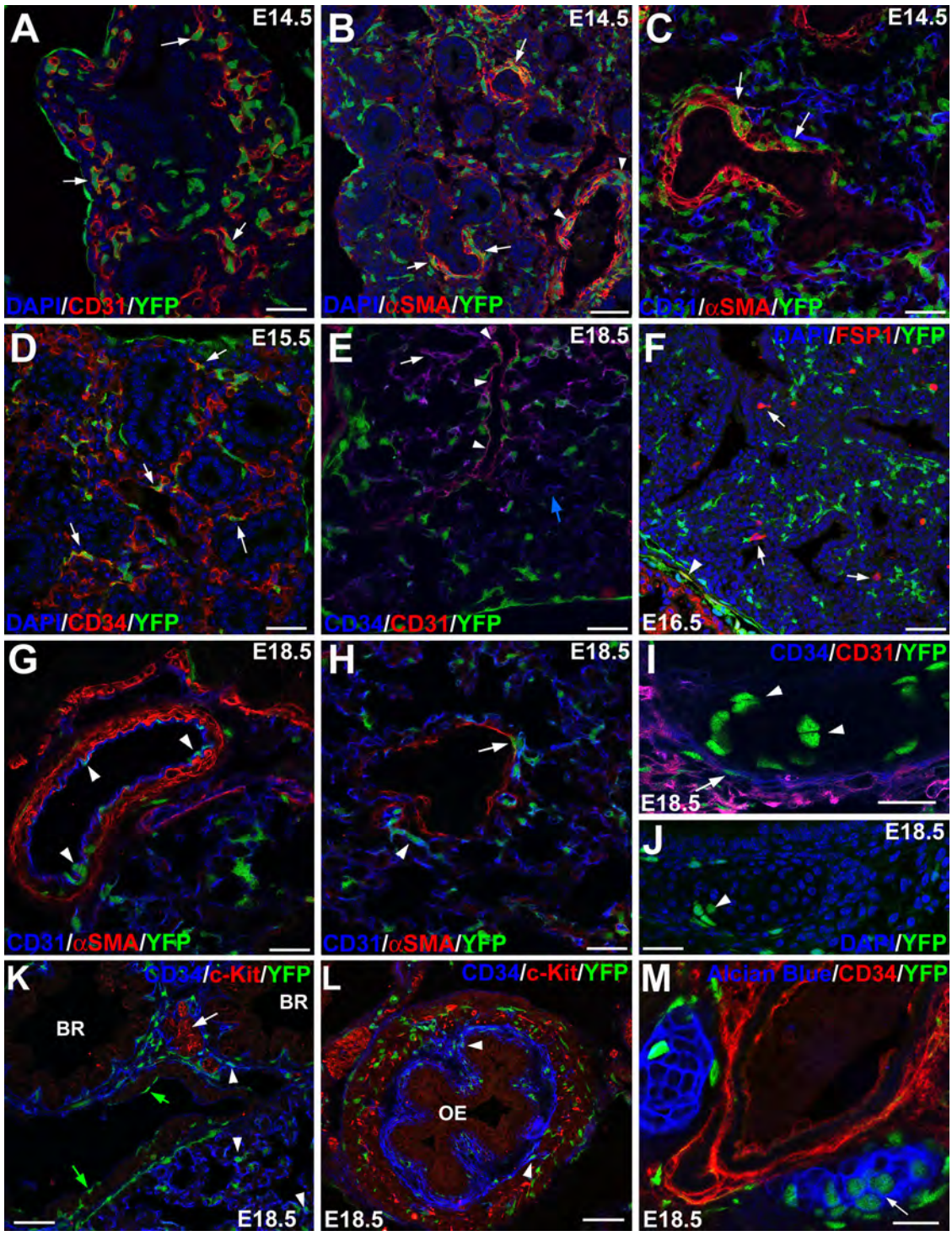

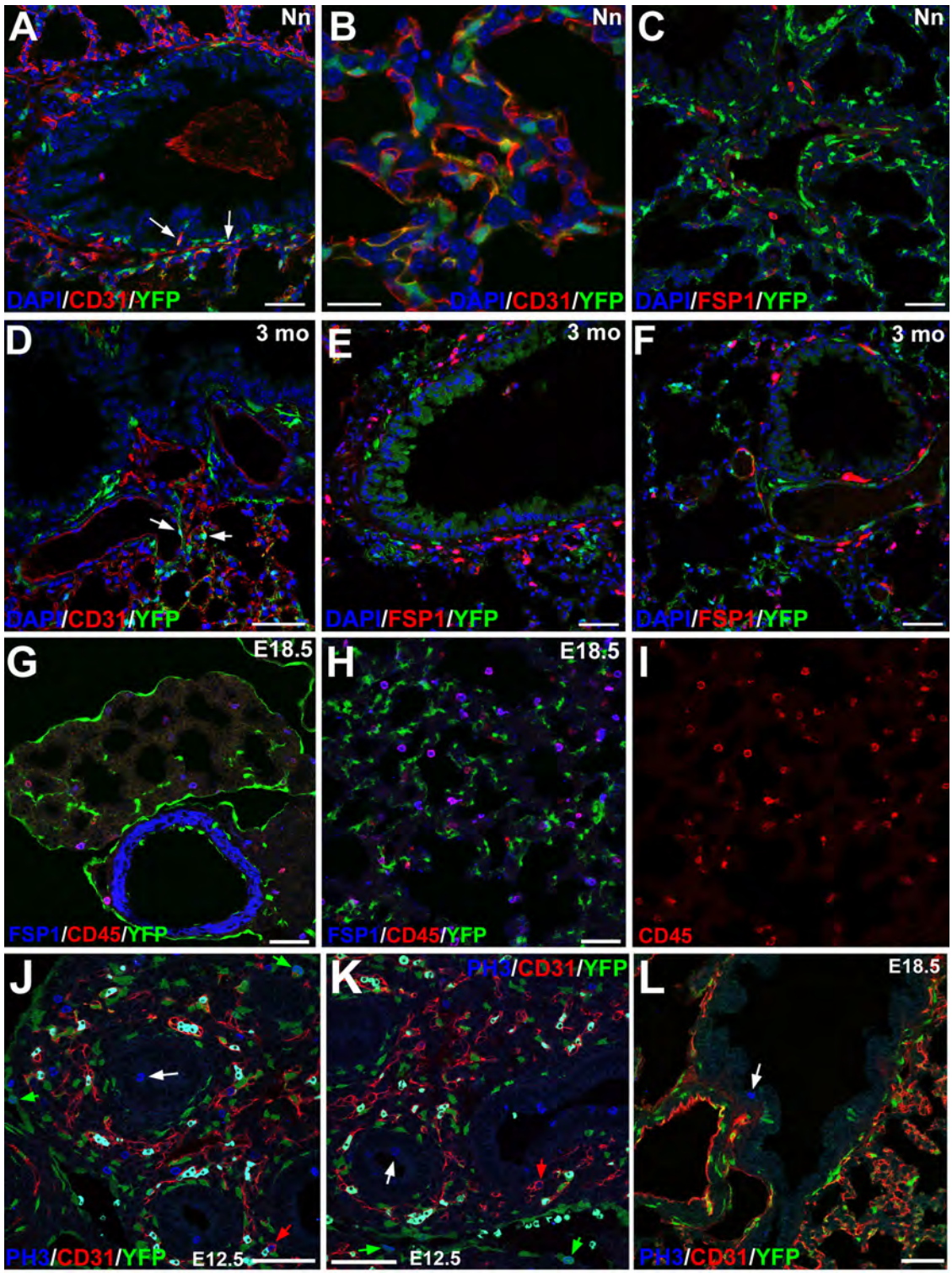

Fig. 4. Cells from the Wt1 lineage are observed in postnatal stages of $Wt1^{cre}$ × ROSA26R-YFP mice. *A* and *B*: $Wt1^{cre}$-YFP cells are abundant in the lungs of these neonate (Nn) mice, where colocalization with CD31 is evident (arrows). *C*: FSP1-positive fibroblasts are present in the lungs of a neonate, but colocalization with YFP is not observed. *D*: abundance of $CD31^+$ cells in an adult (3 mo), where colocalization with YFP is observed (arrows). *E* and *F*: FSP1-positive fibroblasts are abundant in the lungs of this 3-mo-old mouse, but colocalization with YFP is not observed. *G–I*: immunolocalization of FSP1 and the common leukocyte antigen CD45 in the lungs of E18.5 embryos. A large artery with $FSP1^+$ tunica media is shown in *G*. Colocalization of CD45 and FSP1 is evident in most isolated cells. The red channel (CD45) corresponding to *H* is shown in *I*. Note the lack of colocalization of YFP with FSP1 and CD45. *J–L*: immunolocalization of the mitosis marker PH3 in E12.5 (*J* and *K*) and E18.5 (*L*) embryos. In the E12.5 embryo, mitotic YFP^+ cells (green arrows) are located mainly in the mesothelium. Some endothelial cells (red arrows) and endodermal cells (white arrows) are also dividing. However, $PH3^+$ cells are scarce in the E18.5 lungs (*L*). Scale bars = 50 μm, except for *B* (20 μm).

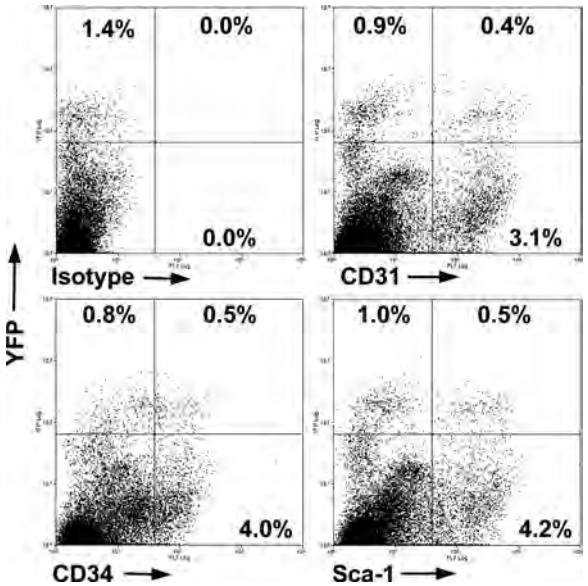

Fig. 5. Flow cytometry analysis of dissociated neonate lungs. *A*: isotype control; 1.4% of all the cells from the lungs are Wt1^{cre}-YFP. *B*: more than a third of the Wt1^{cre}-YFP cells express the CD31 marker. Wt1^{cre}-YFP cells account for a 11% of all the CD31^{+} population. *C*: more than a half of the Wt1^{cre}-YFP cells are CD34^{+}. Again, Wt1^{cre}-YFP account for ~11% of the total CD34^{+} cell population of the lungs. *D*: similar percentages were found for the Sca-1 antigen, a marker that is expressed by pulmonary microvascular endothelial cells during development.

neural tissue was similar in mutant and in control embryos (Fig. 6, *J–M*).

DISCUSSION

Although it had been already shown that the *Wt1* gene is involved in the development of many organs (14, 19, 21, 25, 28), no information was hitherto available about the role played by Wt1 in lung development. The specific expression site of Wt1 is the mesothelium lining the pulmonary sacs, as shown by previous reports (35) and confirmed by our results. Thus Wt1 is a reliable marker of the cells delaminated from the mesothelium through an epithelial-mesenchymal transition. The contribution of cells from the Wt1 lineage cells to the embryonic lung had been previously demonstrated by using a Wt1^{cre} transgenic mouse line (35), but only the origin of pulmonary vascular smooth muscle and a mesenchymal cell population from Wt1-expressing cell lineage could be demonstrated in this report.

The pulmonary mesenchyme, therefore, has a dual origin, from the preexisting, non-Wt1-expressing splanchnopleural mesoderm that surrounds the endodermal sprouts and from the Wt1-expressing mesothelium. We have herein shown evidence that this second population is quantitatively relevant and it has a much wider differentiation potential than previously described. This potential included endothelium, smooth muscle from vessels and bronchia, CD34^{+} fibroblast-like cells, and tracheal/bronchial cartilage. As far as we know, this is the first time that chondrocytes are shown to derive from Wt1-expressing, mesothelium-derived cells. Our findings emphasize the wide potential of differentiation of the mesothelial-derived cells, possibly related with the gain of multipotentiality after an epithelial-mesenchymal transition (4).

Lung bud development in mice begins at E9.5 (9), and we have already found Wt1^{cre}-YFP cells by the stage E10.5, when Wt1 is already strongly expressed in the mesothelium lining the lung primordia. Since the earliest stages of development we can observe the presence of Wt1^{cre}-YFP forming part of the early vascular plexus, expressing the endothelial cell marker CD31 (PECAM-1). Moreover, Wt1^{cre}-YFP cells also express CD34, another marker of the developing endothelium. Pulmonary vasculogenesis occurs by assemblage of progenitors residing in the pulmonary mesenchyme (1, 13). We have demonstrated that two different components (splanchnopleural and mesothelium-derived) contribute to these progenitors. Although the abundance of Wt1^{cre}-YFP cells peaks by midgestation (especially by E16.5) and declines by the end of gestation, our flow cytometry analysis shows that even in neonates Wt1^{cre}-YFP cells still account for more than 3% of all the pulmonary endothelial cells as demonstrated by colocalization of CD31 and Sca-1 with YFP. It is important to remark that Sca-1 is expressed in pulmonary endothelial cells of the mice (20). The decrease of the abundance of the YFP^{+} endothelium during the late gestation cannot be attributed to an increased proliferation of the YFP^{-} endothelium, according to the low levels of mitotic endothelial cells found in E18.5 embryos. Thus we think that recruitment of circulating endothelial progenitors and/or YFP-negative mesenchymal angioblasts might be a source of new endothelial cells in the developing lung vasculature, diluting the original Wt1^{cre}-YFP population.

In late gestational stages, CD34 expression is observed in CD31-negative, fibroblast-like cells, with long prolongations. These CD34^{+} cells have been called "telocytes," and they had been described in the trachea and lungs (16, 34, 44). However, different from what has been described for telocytes, we could not find c-Kit expression in these CD34^{+} cells. We think that the pulmonary CD34^{+} cells are the same interstitial fibroblast-like cells described in other parts of the gastrointestinal tract (33, 39), whose function is still poorly known and deserves further study. The abundance of Wt1^{cre}-YFP cells within this CD34^{+} population suggests that this is a main fate for the mesothelium-derived cells.

Isolated, fibroblast-like FSP1-expressing cells were negative for YFP. This was a surprising observation, given the wide differentiation potential of the Wt1^{cre}-YFP cells, similar to that of the splanchnopleural mesenchyme. We have obtained the same result in intestinal Wt1^{cre}-YFP cells (7). The colocalization of FSP1 with the leukocyte common antigen CD45 suggests that these cells could originate from circulating progenitors of hematopoietic origin. Origin of fibroblasts from circulating cells (a cell type also known as fibrocyte) has been extensively described in processes of fibrosis and scarring (15), being involved in pulmonary fibrosis (2). Our results show that a fibrocyte population could already populate the lung in late fetal stages.

Given the importance of the epithelial-mesenchymal interplay in pulmonary development, and also the quantitative importance of the mesothelium-derived compartment of the lung mesenchyme, the normal development of the lungs might be dependent on the expression of Wt1. Interestingly, a case of bilateral renal agenesis, cardiac defects, and congenital pulmonary airway malformation in a human fetus has been associated with abnormal expression of Wt1 (24). The pulmonary phenotype of the Wt1$^{-/-}$ mouse embryos supports a previously

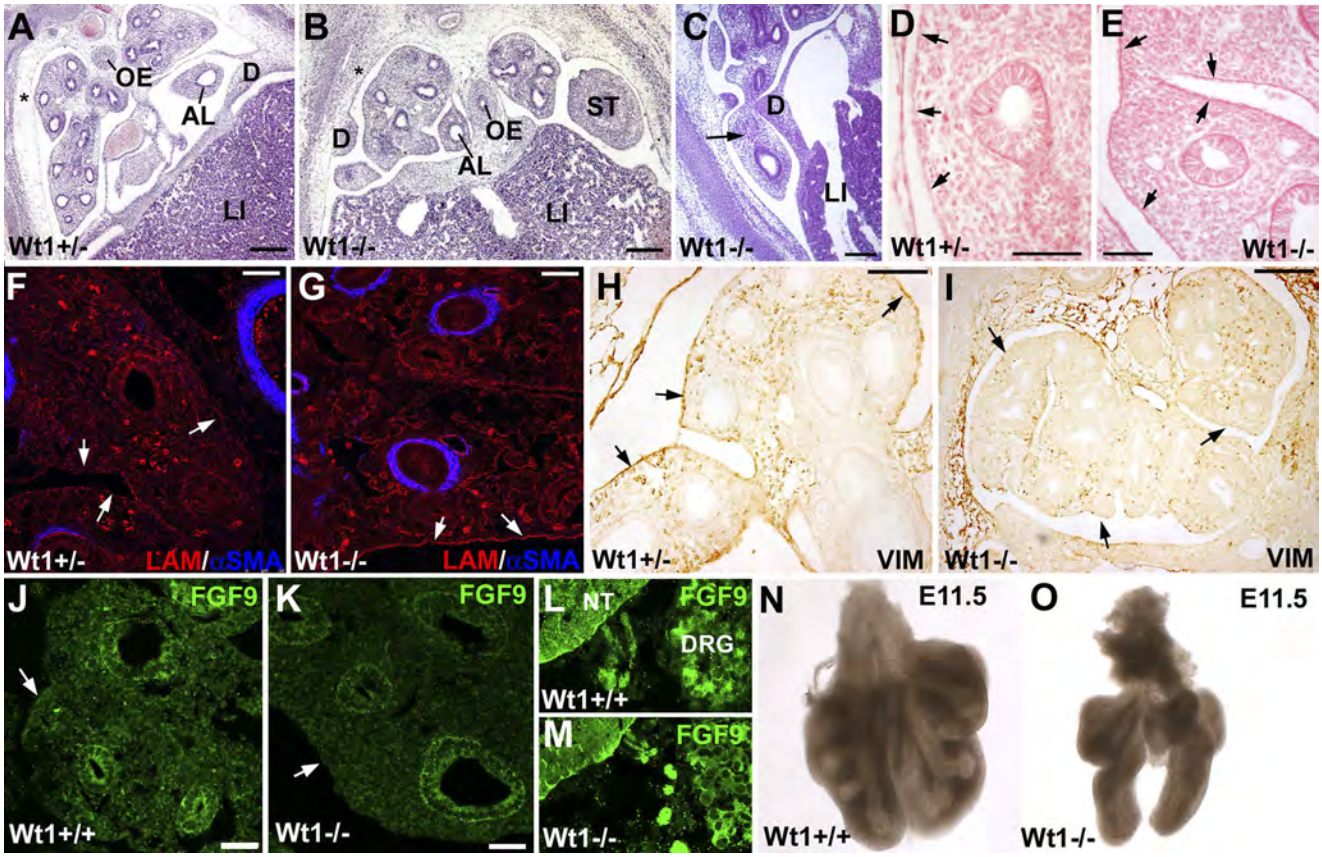

Fig. 6. Pulmonary phenotype in Wt1$^{-/-}$ embryos. *A* and *B*: lungs in a heterozygous control (*A*) and in a Wt1$^{-/-}$ E13.5 embryo (*B*). Lungs from the Wt1$^{-/-}$ embryo show round-shaped, fused lobes, with the accessory lobe (AL) abnormally located in the right pleural cavity. The diaphragm (D) is defective and the pleural cavity is open to the coelomic cavity. The stomach (ST) is in contact with the left lung. The lateral walls of the pleural cavities are abnormally cellularized, whereas these walls in the control embryo are constituted of a loose, poorly cellularized tissue (asterisks). LI, liver. *C*: pulmonary hernia in a Wt1$^{-/-}$ E13.5 embryo. The defective diaphragm has strangled the right pulmonary lobe. *D* and *E*: Sirius red staining in a heterozygous control (*D*) and in a Wt1$^{-/-}$ E13.5 embryo (*E*). A complete basal lamina is present in the mutant embryo (arrows). *F* and *G*: laminin immunoreactivity (in red) also shows a continuous and well-developed basal lamina in the mutant embryo (arrows in *G*), whereas laminin immunoreactivity is discontinuous and weak in the basal surface of the coelomic epithelium of the control (arrows in *F*). No differences are evident in the smooth muscle cells (blue). *H* and *I*: immunolocalization of the mesenchymal marker vimentin shows a reduced number of vimentin-positive cells in the lungs of the mutant (*I*) compared with the control (*H*). Note the vimentin immunoreactivity of the coelomic epithelium of the control (arrows in *H*), whereas the coelomic epithelium of the Wt1$^{-/-}$ lungs is negative for vimentin (arrows in *I*). *J–M*: immunolocalization of FGF9 in control (*J*) and Wt1$^{-/-}$ (*K*) E12.5 embryos. FGF9 immunoreactivity is lower in the pulmonary mesenchyme and particularly in the mesothelium (arrows). However, the FGF9 immunoreactivity in the endodermal epithelium and in the neural tissue (*L* and *M*) is similar in control and mutant embryos. NT, neural tube; DRG, dorsal root ganglion. *N* and *O*: isolated lungs of control and Wt1$^{-/-}$ E11.5 embryos. Mutant lung lobes are narrower and show abnormal lobe anatomy. Scale bars = 25 μm, except for *A–C* (100 μm).

undescribed role for this gene in lung morphogenesis. The anomalies found were mainly related to the shape and arrangement of the pulmonary lobes, which appeared rounded in transverse section and abnormally fused. Pleural cavities were abnormal in size and shape and widely open to the peritoneal cavity because of a diaphragmatic defect. We think that the epithelial-mesenchymal transition of the Wt1-null mesothelium is defective, as suggested by the premature formation of a basal lamina, the lack of vimentin immunoreactivity in the epithelial lining, and the decrease in the number of vimentin-expressing mesenchymal cells in the mutant lungs. Vimentin immunoreactivity of the normal mesothelium is an indicative of an active epithelial-mesenchymal transition (31). This immunoreactivity was not detected in the mesothelium of the mutant. The existence of a strong basal laminin immmunoreactivity in the mutant coelomic epithelium by the stage E13.5 also supports a delayed or blocked contribution of mesothelium-derived cells to the pulmonary mesenchyme, since epithelial-mesenchymal transition involves degradation of the basal lamina. Anyhow, the contribution of the mesothelium-derived cells by this stage is still limited, according our data. For this reason, we cannot discard that most of the anomalies found in the lungs can be secondary to an abnormal development of the pleural cavities, whose walls in Wt1$^{-/-}$ embryos show an abundant cell population instead of the loose, poorly cellularized tissue noticeable in control embryos. The involvement of Wt1 for the development of the subcoelomic mesenchyme and the coelomic septa has been described (29). The excessive cellularization of the pleural walls (where Wt1 is also expressed) can be related with a defective growth of the pleural cavities, thus affecting indirectly to the morphogenesis of the lung lobes. An additional factor to account for the abnormal development of the lungs in the Wt1$^{-/-}$ embryo might be the downregulation of FGF9 expression in the mesothelium and mesenchyme, although expression in the mutant endoderm, where Wt1 is not expressed, is normal.

In conclusion, our results provide novel data on the heterogeneity and the different developmental origin of the mesenchymal cells involved in lung morphogenesis in mammals, and this could be useful in terms of understanding mesenchymal-epithelial interactions during pulmonary development as well as congenital pulmonary defects including diaphragmatic hernia. The potential of the adult pulmonary mesothelium as a source of progenitors in cell therapy of pulmonary diseases is an open question, given the stem cell-like differentiation potential of the embryonic mesothelium-derived cells that we have herein shown. In a closely related case, such as the potential of the adult cardiac mesothelium (i.e., the epicardium), recent results have attracted attention on this possibility (22).

ACKNOWLEDGMENTS

We thank Dr. N. Hastie (University of Edinburgh) for the gift of the $Wt1^{-/-}$, Wt1 GFP/$^{+}$, and Wt470LacZ embryos; Dr. John Burch (National Institutes of Health) for the $Wt1^{cre}$ line; and Dr. Eric G. Neilson (Vanderbilt University School of Medicine, Nashville, TN) for the anti-FSP1 antibody. We also thank David Navas (SCAI, University of Málaga) for technical help with confocal microscopy and flow cytometry.

GRANTS

This work was supported by grants BFU2011-25304 (Ministerio de Economía y Competitividad), P11-CTS-7564 (Junta de Andalucía), and RD12/00190/0022 (TerCel network, ISCIII). E. Cano is recipient of a MINECO fellowship (BES-2009-014847).

DISCLOSURES

No conflicts of interest, financial or otherwise, are declared by the author(s).

AUTHOR CONTRIBUTIONS

E.C. and R.C. performed experiments; E.C., R.C., and R.M.-C. analyzed data; E.C., R.C., and R.M.-C. interpreted results of experiments; E.C. and R.C. drafted manuscript; E.C., R.C., and R.M.-C. edited and revised manuscript; E.C., R.C., and R.M.-C. approved final version of manuscript; R.M.-C. conception and design of research.

REFERENCES

1. **Akeson AL, Wetzel B, Thompson FY, Brooks SK, Paradis H, Gendron RL, Greenberg JM.** Embryonic vasculogenesis by endothelial precursor cells derived from lung mesenchyme. *Dev Dyn* 11: 11–23, 2000.
2. **Andersson-Sjöland A, Nihlberg K, Eriksson L, Bjermer L, Westergren-Thorsson G.** Fibrocytes and the tissue niche in lung repair. *Respir Res* 12: 76, 2011.
3. **Barnes PJ.** Cytokine modulators as novel therapies for airway disease. *Eur Respir J Suppl* 34: 67–77, 2001.
4. **Battula VL, Evans KW, Hollier BG, Shi Y, Marini FC, Ayyanan A, Wang RY, Brisken C, Guerra R, Andreeff M, Mani SA.** Epithelial-mesenchymal transition-derived cells exhibit multilineage differentiation potential similar to mesenchymal stem cells. *Stem Cells* 28: 1435–1445, 2010.
5. **Bellusci S, Grindley J, Emoto H, Itoh N, Hogan BL.** Fibroblast growth factor 10 (FGF10) and branching morphogenesis in the embryonic mouse lung. *Development* 124: 4867–4878, 1997.
6. **Cardoso WV.** Molecular regulation of lung development. *Annu Rev Physiol* 63: 471–494, 2001.
7. **Carmona R, Cano E, Mattiotti A, Gaztambide J, Muñoz-Chápuli R.** Cells derived from the coelomic epithelium contribute to multiple gastrointestinal tissues in mouse embryos. *PLoS One* 8: e55890, 2013.
8. **Colvin JS, White AC, Pratt SJ, Ornitz DM.** Lung hypoplasia and neonatal death in Fgf9-null mice identify this gene as an essential regulator of lung mesenchyme. *Development* 128: 2095–2106, 2001.
9. **Costa RH, Kalinichenko VV, Lim L.** Transcription factors in mouse lung development and function. *Am J Physiol Lung Cell Mol Physiol* 280: L823–L838, 2001.

9a. **del Monte G, Casanova JC, Guadix JA, MacGrogan D, Burch JB, Pérez-Pomares JM, de la Pompa JL.** Differential Notch signaling in the epicardium is required for cardiac inflow development and coronary vessel morphogenesis. *Circ Res* 108: 824–836, 2011.

10. **de Mello DE, Sawyer D, Galvin N, Reid LM.** Early fetal development of lung vasculature. *Am J Respir Cell Mol Biol* 16: 568–581, 1997.
11. **de Mello DE, Reid LM.** Embryonic and early fetal development of human lung vasculature and its functional implications. *Pediatr Dev Pathol* 3: 439–449, 2000.
12. **Duman-Schel M, Weng L, Xin S, Du W.** Hedgehog regulates cell growth and proliferation by inducing Cyclin D and Cyclin E. *Nature* 417: 299–304, 2002.
13. **Gebb SA, Shannon JM.** Tissue interactions mediate early events in pulmonary vasculogenesis. *Dev Dyn* 217: 159–169, 2000.
14. **Herzer U, Crocoll A, Barton D, Howells N, Englert C.** The Wilms tumor suppressor gene wt1 is required for development of the spleen. *Curr Biol* 12: 837–840, 1999.
15. **Herzog EL, Bucala R.** Fibrocytes in health and disease. *Exp Hematol* 38: 548–556, 2010.
16. **Hinescu ME, Gherghiceanu M, Suciu L, Popescu LM.** Telocytes in pleura: two- and three-dimensional imaging by transmission electron microscopy. *Cell Tissue Res* 343: 389–397, 2011.
17. **Hogan BL.** Morphogenesis. *Cell* 96: 225–233, 1999.
18. **Hosen N, Shirakata T, Nishida S, Yanagihara M, Tsuboi A, Kawakami M, Oji Y, Oka Y, Okabe M, Tan B, Sugiyama H, Weissman IL.** The Wilms' tumor gene WT1-GFP knock-in mouse reveals the dynamic regulation of WT1 expression in normal and leukemic hematopoiesis. *Leukemia* 21: 1783–1791, 2007.
19. **Ijpenberg A, Pérez-Pomares JM, Guadix JA, Carmona R, Portillo-Sánchez V, Macías D, Hohenstein P, Miles CM, Hastie ND, Muñoz-Chápuli R.** Wt1 and retinoic acid signaling are essential for stellate cell development and liver morphogenesis. *Dev Biol* 312: 157–170, 2007.
20. **Kotton DN, Summer RS, Sun X, Ma BY, Fine A.** Stem cell antigen-1 expression in the pulmonary vascular endothelium. *Am J Physiol Lung Cell Mol Physiol* 284: L990–L996, 2003.
21. **Kreidberg JA, Sariola H, Loring JM, Maeda M, Pelletier J, Housman D, Jaenisch R.** WT-1 is required for early kidney development. *Cell* 74: 679–691, 1993.
22. **Limana F, Capogrossi MC, Germani A.** The epicardium in cardiac repair: from the stem cell view. *Pharmacol Ther* 129: 82–96, 2011.
23. **Long F, Zhang XM, Karp S, Yang Y, McMahon AP.** Genetic manipulation of hedgehog signaling in the endochondral skeleton reveals a direct role in the regulation of chondrocyte proliferation. *Development* 128: 5099–5108, 2001.
24. **Loo CK, Pereira TN, Ramm GA.** Abnormal WT1 expression in human fetuses with bilateral renal agenesis and cardiac malformations. *Birth Defects Res A Clin Mol Teratol* 94: 116–122, 2012.
25. **Martínez-Estrada OM, Lettice LA, Essafi A, Guadix JA, Slight J, Velecela V, Hall E, Reichmann J, Devenney PS, Hohenstein P, Hosen N, Hill RE, Muñoz-Chapuli R, Hastie ND.** Wt1 is required for cardiovascular progenitor cell formation through transcriptional control of Snail and E-cadherin. *Nat Genet* 42: 89–93, 2010.
26. **Min H, Danilenko DM, Scully SA, Bolon B, Ring BD, Tarpley JE, DeRose M, Simonet WS.** Fgf-10 is required for both limb and lung development and exhibits striking functional similarity to Drosophila branchless. *Genes Dev* 12: 3156–3161, 1998.
28. **Moore AW, McInnes L, Kreidberg J, Hastie ND, Schedl A.** YAC complementation shows a requirement for Wt1 in the development of epicardium, adrenal gland and throughout nephrogenesis. *Development* 126: 1845–1857, 1999.
29. **Norden J, Grieskamp T, Lausch E, van Wijk B, van den Hoff MJ, Englert C, Petry M, Mommersteeg MT, Christoffels VM, Niederreither K, Kispert A.** Wt1 and retinoic acid signaling in the subcoelomic mesenchyme control the development of the pleuropericardial membranes and the sinus horns. *Circ Res* 106: 1212–1220, 2010.
30. **Parera MC, van Dooren M, van Kempen M, de Krijger R, Grosveld F, Tibboel D, Rottier R.** Distal angiogenesis: a new concept for lung vascular morphogenesis. *Am J Physiol Lung Cell Mol Physiol* 288: L141–L149, 2005.
31. **Pérez-Pomares JM, Macías D, García-Garrido L, Muñoz-Chápuli R.** Contribution of the primitive epicardium to the subepicardial mesenchyme in hamster and chick embryos. *Dev Dyn* 210: 96–105, 1997.
32. **Pérez-Pomares JM, Macías D, García-Garrido L, Muñoz-Chápuli R.** The origin of the subepicardial mesenchyme in the avian embryo: an immunohistochemical and quail-chick chimera study. *Dev Biol* 200: 57–68, 1998.

33. **Pieri L, Vannucchi MG, Faussone-Pellegrini MS.** Histochemical and ultrastructural characteristics of an interstitial cell type different from ICC and resident in the muscle coat of human gut. *J Cell Mol Med* 12: 1944–1955, 2008.
34. **Popescu LM, Gherghiceanu M, Suciu LC, Manole CG, Hinescu ME.** Telocytes and putative stem cells in the lungs: electron microscopy, electron tomography and laser scanning microscopy. *Cell Tissue Res* 345: 391–403, 2011.
35. **Que J, Wilm B, Hasegawa H, Wang F, Bader D, Hogan BL.** Mesothelium contributes to vascular smooth muscle and mesenchyme during lung development. *Proc Natl Acad Sci USA* 105: 16626–16630, 2008.
36. **Schachtner SK, Wang Y, Scott Baldwin H.** Qualitative and quantitative analysis of embryonic pulmonary vessel formation. *Am J Respir Cell Mol Biol* 22: 157–165, 2000.
37. **Sekine K, Ohuchi H, Fujiwara M, Yamasaki M, Yoshizawa T, Sato T, Yagishita N, Matsui DK, Itoh N, Kato.** FgF-10 is essential for limb and lung formation. *Nat Genet* 21: 138–141, 1999.
38. **Shannon JM.** Induction of alveolar type II cell differentiation in fetal tracheal epithelium by grafted distal lung mesenchyme. *Dev Biol* 166: 600–614, 1994.
39. **Vanderwinden JM, Gillard K, De Laet MH, Messam CA, Schiffmann SN.** Distribution of the intermediate filament nestin in the muscularis propria of the human gastrointestinal tract. *Cell Tissue Res* 309: 261–268, 2002.
40. **Warburton D, Shwart M, Teff D, Flores-Delgado G, Anderson KD, Cardoso WV.** The molecular basis of lung morphogenesis. *Mech Dev* 92: 55–81, 2000.
41. **Weaver M, Dunn NR, Hogan BL.** Bmp4 and Fgf10 play opposing roles during lung bud morphogenesis. *Development* 127: 2695–2704, 2000.
42. **Wessels A, van den Hoff MJ, Adamo RF, Phelps AL, Lockhart MM, Sauls K, Briggs LE, Norris RA, van Wijk B, Perez-Pomares JM, Dettman RW, Burch JB.** Epicardially derived fibroblasts preferentially contribute to the parietal leaflets of the atrioventricular valves in the murine heart. *Dev Biol* 366: 111–124, 2012.
43. **White AC, Xu J, Yin Y, Smith C, Schmid G, Ornitz DM.** FGF9 and Shh signaling coordinate lung growth and development through regulation of distinct mesenchymal domains. *Development* 133: 1507–1517, 2006.
44. **Zheng Y, Li H, Manole CG, Sun A, Ge J, Wang X.** Telocytes in trachea and lungs. *J Cell Mol Med* 15: 2262–2268, 2011.